Effects of *SDHD* H50R Missense Mutation on Thyroid Tumorigenesis

Undergraduate Honors Research Thesis

Presented in Partial Fulfilllment of the Requirements of Graduation with Research Distinction in Biomedical Science in the College of Medicine at The Ohio State University

By

Karthik Chakravarthy

The Ohio State University

April 2019

Project Advisor: Dr. Lawrence S. Kirschner, Department of Internal Medicine, Division of Endocrinology, Diabetes, and Metabolism

Table of Contents

Introduction

Thyroid cancer is among the most common cancers and is the most frequent type of endocrine malignancy (Kirschner et al., 2016). It has also been increasing in prevalence over the past decade (Davies et al., 2015). Increased risk of thyroid cancer has been associated with Cowden syndrome (CS), which is an inherited endocrine tumor disorder. CS is characterized by the presence of small tumor-like growths, known as hamartomas, and has been found to provide an increased risk of the development of other tumors (Nagy et al., 2004). Germline mutations in the phosphatase and tensin homolog (*PTEN*) tumor suppressor gene have been shown to cause CS and are identified in 85% of CS-associated and 10% of sporadic thyroid cancers (Yeager et al., 2007). In addition, germline variations in the succinate dehydrogenase complex (*SDH*) genes, which were first identified as tumor suppressor genes in patients with pheochromocytoma and paraganglioma, have been recently discovered in CS patients with thyroid cancer (Ni et al., 2008). Physiologically, SDH functions in the citric acid cycle where it catalyzes the conversion of succinate to fumarate within the mitochondrial intermembrane space, and thus plays a crucial role in metabolic processes (Cantor et al., 2012). Activation and induction of carcinogenic cellular environment can occur through changes in metabolic pathways involving a shift from aerobic respiration to anaerobic glycolysis, which is known as the Warburg effect (Cantor et al., 2012). These changes could potentially be caused by alterations in genes coding for mitochondrial enzymes, such as SDH, consequently impacting normal cellular metabolism and leading to cancerous effects (Cantor et al., 2012).

SDH is composed of four protein subunits (A, B, C, and D), of which succinate dehydrogenase subunit D (*SDHD*) gene possesses a relatively high frequency of germline variations found within the patient population, thus making it a gene of interest within this study

(Bayley et al., 2005). Studies have shown that CS patients with variations in the *SDHD* gene either alone or in combination with *PTEN* mutations display an increased risk for thyroid as well as breast cancers in comparison to CS patients with only *PTEN* mutations (Ni et al., 2012). Hence, changes in *SDHD* functionality due to genetic variations may confer a unique thyroid-specific effect leading to the greater tumor progression observed within those patients with alterations in the *SDHD* gene.

Previous studies from the Kirschner Lab examining tumor development within the thyroid glands compared thyroid-specific *Sdhd* deletion and thyroid-specific *Sdhd/Pten* deletion experimental models to *Sdhd*-wildtype and thyroid-specific *Pten* deletion control models, respectively. Based on ultrasound imaging of thyroid glands and histopathological staining of follicular regions, *Sdhd*-null models were found to display larger thyroid volumes, and along with *Sdhd/Pten*-null models exhibited decreased follicle area, and increased cell density and proliferation; however, Sdhd/Pten-null models displayed actual tumors more often than Sdhd-null models

Studies examining germline variations in *SDHD* have identified the His50Arg (H50R) variation as being associated more frequently with sporadic thyroid tumor cases in patients both with and without the presence of a *PTEN* mutation (Bardellae et al., 2011). The H50R genetic alteration is caused by a missense mutation involving a single nucleotide change that results in the mRNA codon translating for the amino acid arginine instead of the amino acid histidine. While frequent mutations can be identified within human cancer patients, the manner with which these mutations can lead to the development of such tumor disorders may not be fully understood. Specifically, it is unknown whether missense mutations in *SDHD* produce tumorigenic effects within the thyroid glands, as well as how these tumors might occur.

Therefore, it is essential to model this tumor progression in vivo to better understand how such mutations in the human patient population lead to thyroid and other cancers.

The hypothesis for this research study is that *Sdhd* H50R mutant allele will promote tumorigenesis and lead to the development of tumors within the murine thyroid. Patients with this missense mutation have been shown to have greater incidence of thyroid cancers and display downstream effects on targets commonly found in tumorigenic pathways. Since *SDHD* has been identified as a tumor suppressor in other endocrine tumor disorders, it is expected that the tumorigenesis resulting from H50R mutation will be due to the loss of *Sdhd* function caused by the genetic alteration, acting as an impetus for the thyroid tumor development.

Materials and Methods

As the research project focuses on examining the effects of the $Sdhd^{H50R}$ mutation on thyroid tumorigenesis, the experimental design will focus on characterizing these effects through methods that assess gross anatomical changes, histological alterations on a cellular level, and the potential effect on sub-cellular processes including metabolism. This will be able to provide a holistic picture of the impact that the $Sdhd^{H50R}$ mutation has regarding multiple stages of tumor progression in the thyroid glands.

Animal Strains, Husbandry and Maintenance

The use of animals complied with federal and The Ohio State University Laboratory Animal Resources regulations (IACUC Protocol # 2009A0084-R3). Mouse models with thyroid-specific *Sdhd* deletion and/or *Sdhd* H50R mutation were generated, using CRISPR-Cas9 genome editing to generate a heterozygous *Sdhd* H50R mutant founder. Several generations of breeding between the founder and a mouse with thyroid-specific *Sdhd* deletion produced *Sdhd* H50R

mutation (*Sdhd*$^{H50R/Wt}$), homozygous *Sdhd* mutation (*Sdhd*$^{H50R/H50R}$), and heterozygous *Sdhd* H50R mutation with thyroid-specific deletion of the non-mutant *Sdhd* allele (*Tpo-Sdhd*$^{H50R/-}$), also referred to as hemizygous *Sdhd* H50R. Control mouse models (generated within the same cohorts as the experimental models) included thyroid-specific *Sdhd* deletion (*Tpo-Sdhd*$^{-/-}$) as a positive control and wildtype *Sdhd* (*Sdhd*$^{Wt/Wt}$) as a negative control. The experiments were performed using littermate mice from a mixed C57BL/6 and FVB genetic background.

Genotyping and Sanger Sequencing

Polymerase chain reaction (PCR), conducted using Go-Taq protocol with primers specific for *Sdhd*-lox and TPO-cre, and Sanger Sequencing, performed through the Genomics Shared Resource at The Ohio State University, were utilized to verify the types of *Sdhd* alleles and if the H50R mutation was present in each model.

Survival Analysis

Due to spontaneous early demises occurring among mutant models, date of death of individual mice were noted up to 12 months. This data was plotted on a Kaplan-Meier curve using PRISM software to evaluate the trends in *Sdhd*^{H50R} mutant models' survival.

Body Mass Measurements

Body mass of individual mice was measured after 12 months using a portable weighing scale with accuracy to the nearest tenth of a gram.

Ultrasonography

Mice were imaged with a VisualSonics Vevo 2100 (VisualSonics, Toronto, CA, USA) after 12 months of age. MS550D transducer (22–55 MHz) was used with 3D-mode imaging to determine the size of the thyroid. The volume of both thyroid lobes was calculated using Vevolab 2.1 software in a blinded fashion.

Histology

The hematoxylin and eosin (H&E)-stained sections of thyroid and adrenal glands were processed and produced by the Comparative Pathology Services at The Ohio State University. The samples of thyroid and adrenal glands were imaged at 20× magnification.

Mouse Embryonic Fibroblast (MEF) Isolation and Cell Culture

Mouse embryos were isolated from pregnant females (through *Sdhd*$^{H50R/Wt}$ crossings) and after liver/heart tissue was removed, each embryo was individually chopped using a sterilized blade and digested in 0.25% trypsin-EDTA for a total of 1 hour. Cells were combined with 40 mL of DMEM growth media, centrifuged at 350g for 10 minutes, and the pellet was resuspended in 10 mL of DMEM and plated onto 10 mm diameter plates. Cell lines were cultured for two passages and then frozen at -80°C.

Cell Proliferation/Growth

Twenty thousand cells were plated in 12-well plates for a growth curve by crystal violet assay. At each time point, triplicate wells were stained with 0.05% crystal violet, 0.1% formalin for 20 min and extracted with 10% acetic acid. Absorbance was measured at 590 nm.

Mitochondrial Stress Assay

Seahorse XF Cell Mito Stress Test was used to measure the oxygen consumption rate (OCR) via the Seahorse XF Cell Mito Stress Test Kit and respective Report Generator. MEF cells (*Sdhd*$^{H50R/Wt}$, *Sdhd*$^{H50R/H50R}$, *Sdhd*$^{Wt/Wt}$) were plated at a density of 20,000 cells per well (XF24 cell culture microplate; Seahorse Biosciences, North Billerica, MA, USA). The cells were allowed to grow for 24-hours, following which the cells were washed with XF Assay media (with 20 mM glucose, 1 mM sodium pyruvate, no sodium bicarbonate at pH 7.4). The cells were

incubated for 1 hour at 37°C in a non-CO_2 incubator. The assay was normalized to cell count and analyzed using the XFe24 analyzer and corresponding Wave software.

Results

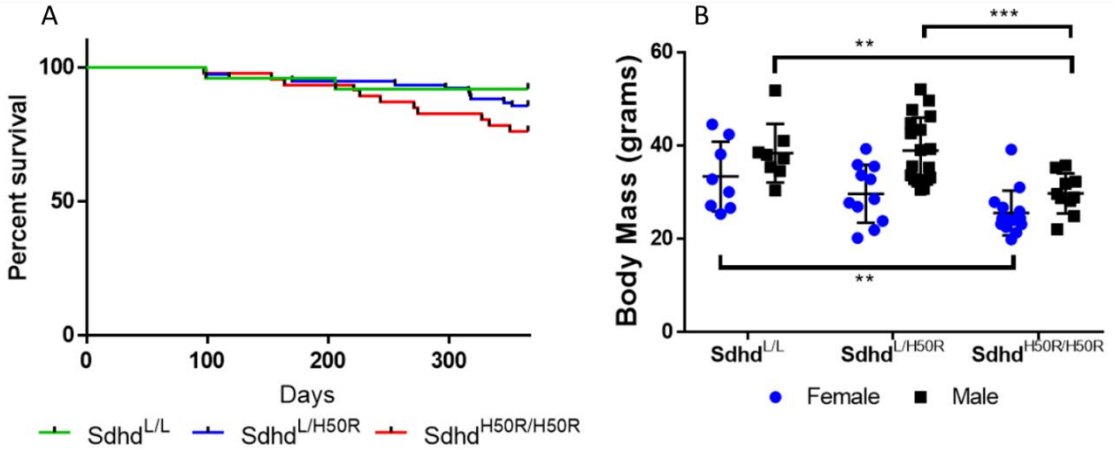

Figure 1: Impact on survival and weight gain for *Sdhd*^{H50R} mutants. *(A) Survival analysis of global H50R homozygous (n=46), heterozygous (n=76), and wildtype mice (n=25). (B) Lower Sdhd$^{H50R/H50R}$ mass.*

<u>*Sdhd*^{h50r} Mutants Demonstrate Changes in Overall Lifespan and Size</u>

Being the first ever global *Sdhd*^{H50R} mutant mouse models, an important query of this project involved examining the potential for embryonic lethality for *Sdhd*^{H50R} mutants, which had been established as a consequence of global ablation of Sdhd in previous mouse models. However, all mice possessing an H50R mutation in this study were found to be embryonically viable and also demonstrated a capacity to reproduce. Yet, it was observed that mice possessing one or two copies of the *Sdhd*^{H50R} allele exhibited lower rates of survival in comparison to the wildtype controls, with the greatest decrease in survival observed after 200 days for *Sdhd$^{H50R/Wt}$* and 300 days for *Sdhd$^{H50R/H50R}$* (Figure 1A). Due to the global *Sdhd*^{H50R} mutation, we were interested in identifying any gross physiological changes in mutant models. When comparing body weight between mutants and wildtype models for both male and female mice, it can be

noted that *Sdhd*$^{H50R/H50R}$ males and females possess significantly lower body weights than the respective *Sdhd*^{H50R} heterozygotes and wildtype models (Figure 1B).

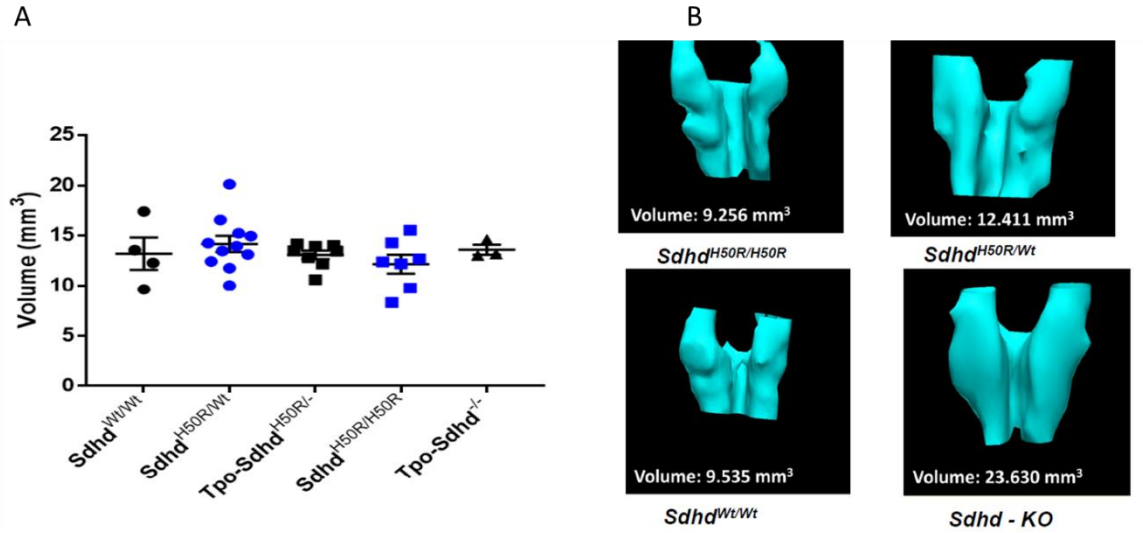

Figure 2: Thyroid volumes are not significantly affected. *(A) Volumes of thyroid glands from experimental and control models at six months of age. (B) Representative 3-D structures and volumes of thyroid glands from experimental and control groups at 12 months of age.*

Sdhd^{H50R} Models Lack Increases in Thyroid Volume

Changes in thyroid volumes can be indicative of initiation of tumorigenesis and also act as a precursor for tumor progression. When comparing thyroid volumes at 6 months of age, it was observed that there was no significant difference between the mutant *Sdhd*^{H50R} models and the controls (Figure 2A). However, at 12 months of age, mouse thyroids of models with homozygous (n=10) and heterozygous *Sdhd*^{H50R} (n=10) mutations were more similar in volume to *Sdhd*-wildtypes (n=5) and in normal physiological range, as compared to *Sdhd*-KO (n=6) controls which had much larger thyroid volumes (Figure 2B).

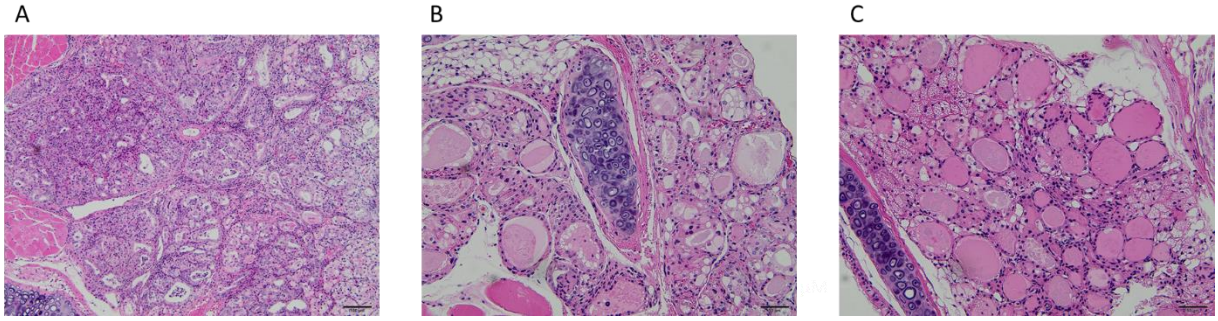

Figure 3: *Sdhd*^{H50R} mutation led to alterations in thyroid follicles. *Representative histological images at 20X magnification for (A) Sdhd^{H50R} homozygous thyroid tissue (n=2), (B) Sdhd^{H50R} heterozygous thyroid tissue (n=3), and (C) Sdhd-wildtype thyroid tissue (n=2).*

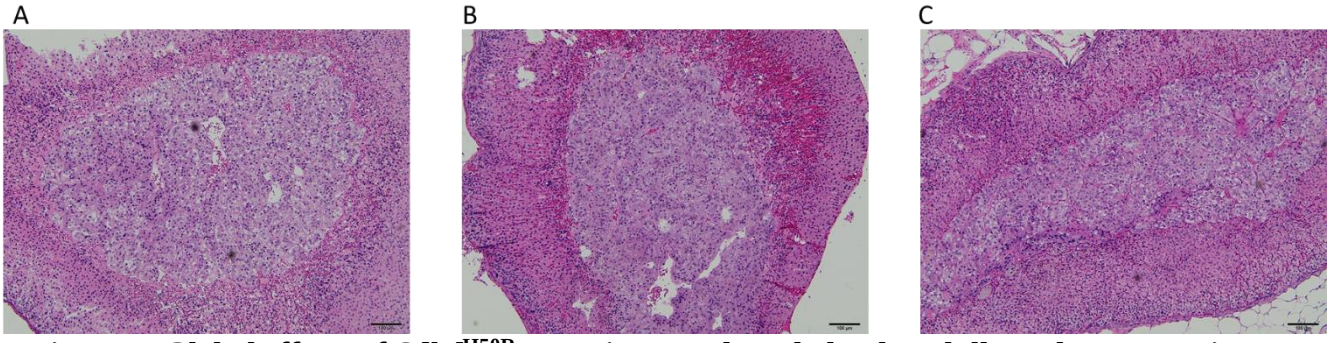

Figure 4: Global effects of *Sdhd*^{H50R} mutation on adrenal gland medulla and cortex regions. *Representative histological images at 20X magnification for (A) Sdhd^{H50R} homozygous adrenal tissue (n=2), (B) Sdhd^{H50R} heterozygous adrenal tissue (n=3), and (C) Sdhd-wildtype adrenal tissue (n=3).*

Follicular Dysplasia Present in *Sdhd*^{H50R} Mutant Tissue

Due to alterations in cellular structure within thyroid tissue being a key component of tumor progression, we examined sections thyroid tissues which revealed that both heterozygous and homozygous mutant models possessed significant changes indicating cellular proliferation and dysplasia surrounding the thyroid follicles in comparison to wildtype models (Figure 3A-3C). Additionally, to the potential effects in other endocrine tissues due to the global nature of

the *Sdhd*^{H50R} mutation, adrenal gland tissues were also studied and revealed changes with cellular proliferation within the regions of cells including the adrenal medulla (Figure 4A-4C).

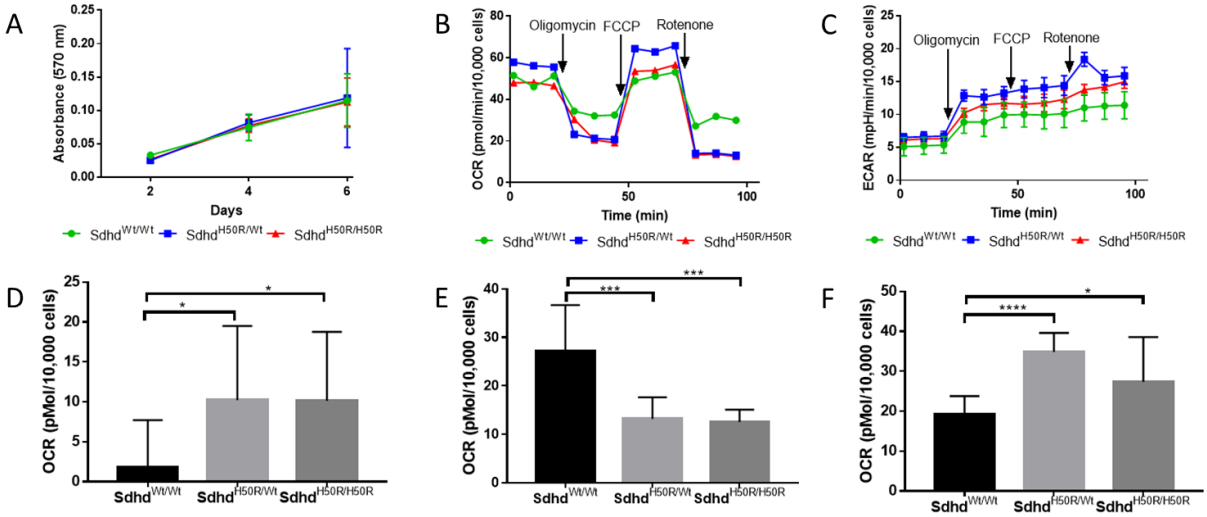

Figure 5: *Sdhd*^{H50R} mutant cells demonstrate variation in cellular energy production despite normal growth over time. *(A) Cellular growth for Sdhd^{H50R} mutant and wildtype cells (Replicates of 10 samples). (B) Mitochondrial function graph for cell lines over stress assay progression. (C) Glycolytic rate for cell lines during stress assay. (D) Spare capacity graph for mutant and wildtype cells. (E) Non-mitochondrial oxygen consumption for mutant and wildtype cells. (F) ATP-production for mutant and wildtype cells.*

H50R Mutation in *Sdhd* Gene Results in Deregulation on Cellular Energetics in MEF Cell Lines

Since the *Sdhd* gene functions within the SDH protein complex in the mitochondria, it was critical to investigate changes caused by the missense mutation that could have affected cellular growth and metabolism and promoted tumor progression. Cellular proliferation assays revealed that there was no significant difference in growth among all the timepoints between cell lines with at least one copy of the H50R mutation and wildtype cells (Figure 5A). However, assessments of mitochondrial function indicated significant differences in mitochondrial function based on trends of oxygen consumption rate (OCR) (Figure 5B). In particular, *Sdhd*^{H50R} mutant cell lines exhibiting statistically significant increases in spare capacity and ATP production values, as well as significant decreases in non-mitochondrial oxygen consumption in comparison

to wildtype cell lines (Figure 5D-5F). Additionally, mutant cell lines also exhibited greater trends in extra-cellular acidification rate (ECAR) values compared to wildtype cells (Figure 5C).

Discussion

While ablation of the *Sdhd* gene in mice has commonly led to certain characteristics indicative of tumorigenic pathways and altered physiological state, this study showed unique effects of the *Sdhd*^{H50R} missense mutation within the murine models. The embryonic viability of mice with global homozygous *Sdhd*^{H50R} alleles demonstrated that the mutation did not have the same developmental defects that occurred among global Sdhd-knockouts. However, despite embryonic viability, *Sdhd*^{H50R} mutant mice displayed lower rates of survival within one year, with discernable trends of lifespan between homozygous, heterozygous, and wildtype models. Given the statistically significant lower body masses among *Sdhd*^{H50R} homozygotes, this indicates a potential global effect that could involve mice wasting away and thus having lower survival rates and body weights. However, since initial dissection studies have revealed that the variation in weight may be largely due to differences in the amount of adipose tissue present in the mice, it could be possible that the mutation may be affecting the overall metabolism in mice and leading to less accumulation of fats and subsequently reducing overall lifespan.

When specifically examining the effects of the missense mutation on the thyroid glands, it was noticed that thyroid volumes for mutant models were smaller compared to KO-models and more similar to wildtype controls after one year. This, along with the lack of significant growth at early timepoints could be indicative that the *Sdhd*^{H50R} mutation may lack the robust phenotype associated with large increases in tumor volume observed with thyroid-specific deletions, and that the effects of the mutation within thyroid gland may be subtler.

Upon looking at the histology of the thyroid gland, it could be identified that severe alterations had been occurring within the follicular regions of the thyroids. The pathology of the thyroid glands for all mouse models revealed that were no tumors present within the thyroid. However, closer analysis of the thyroid tissue revealed dysplasia of follicle areas, with greater cellular proliferation and an observable decrease in the follicular areas in *Sdhd*^{H50R} homozygous and heterozygous models compared to *Sdhd*-wildtype. These cellular changes indicate putative tumor initiation pathways within the thyroid tissue that may be of consequence within the *Sdhd*^{H50R} models despite the normal size of the thyroid glands, indicating a potential restructuring of the thyroid gland that is consistent with initial tumor formation. Increased cellular proliferation also observed in the medulla and cortex boundaries of adrenal glands signified the global physiological impact of the H50R mutation, including affecting other endocrine system organs as well as potential cellular neoplasia within the adrenal glands. These effects observed within the heterozygous mutant mouse may suggest the initiation of tumor development caused by the missense mutation and display potential progression to cancer at further stages.

The cellular data shown in the proliferation assay revealed that despite changes occurring at the tissue level, the overall growth of cells with the *Sdhd*^{H50R} mutation did not differ significantly for cells without the mutation. Upon a closer examination of the mitochondrial function of the cell lines, it was determined that cells possessing at least one copy of the mutant allele demonstrated greater mitochondrial function. This was shown by the elevations in spare capacity and ATP-production, which indicated that cells with the mutation were able to respond to greater metabolic demands and that the overall energetic pathways within the mitochondria had been altered. Furthermore, the lower levels of non-mitochondrial oxygen consumption

revealed the relative high functionality of the mitochondria as well as the fact that oxidation of free radicals and inflammatory biomarkers were reduced. This postulates that there is an increase in mitochondrial activity. Additionally, glycolytic rates, which were indicated by ECAR values, were greater in mutation cell lines compared to wildtype cells. These two findings reveal that while the mutation does not seem to cause the types of metabolic changes associated with the Warburg effect, which include reduced mitochondrial oxidative phosphorylation and increased glycolysis, it can be seen that the mutation does result in a deregulation of cellular energetic pathways and may be the first step in potentially driving metabolism that is more favorable to a tumor environment.

Overall, it was observed that the *Sdhd*^{H50R} mutation resulted in the unique effects, with significant global effects across multiple tissues and yet lacked certain characteristics common to tumor models, given the reduced thyroid volumes and variation from energetic pathways based on the Warburg effect. However, both murine and cellular models with the H50R mutation did demonstrate several aspects of dysregulation and alterations that could be responsible for potential tumor progression. Contrary to the initial hypothesis, *Sdhd*^{H50R} homozygous and heterozygous models demonstrated similar effects, as seen with reduced viability, similar thyroid volumes, tissue dysplasia, and common deregulation of cellular energetics. This may imply that the *Sdhd*^{H50R} mutation may not function completely within a loss-of-function genetic mechanism and could possible have either a gain-of-function effect, given the unique cell metabolism, or even a dominant-negative impact, resulting in similar phenotypes between the *Sdhd*^{H50R} homozygous and heterozygous models. To fully elucidate the nature of this mutation, it would be critical to conduct protein analyses to examine downstream molecular targets within the *Sdhd* and *Pten* signaling pathways, which can be critical for tumor pathways. Additionally, looking

into the certain metabolic byproducts of the Krebs cycle and oxidative phosphorylation chain may also provide insight regarding changes in functionality due to the mutation. Finally, since *Pten* can often alter the effects of the *Sdhd* within a tumor model, it would be essential to create and evaluate mouse models possessing both *Pten*-deletions and $Sdhd^{H50R}$ mutations.

References

1. Kirschner LS, Qamrib Z, Kari S, Ashtekar A. Mouse Models of Thyroid Cancer: A 2015 Update. *Mol Cell Endocrinol*. 2016;421:18–27.
2. Davies L, Morris LG, Haymart M, Chen AY, Goldenberg D, Netterville J, Wong RJ. American Association of Clinical Endocrinologists and American College of Endocrinology disease state clinical review: the increasing incidence of thyroid cancer. *Endocrine Practice.* 2015; 21:686–696.
3. Ni Y, He X, Ringel MD, Eng C. Germline SDHx variants modify breast and thyroid cancer risks in Cowden and Cowden-like syndrome via FAD/NAD-dependant destabilization of p53. *Hum Mol Gen*. 2012;21(2):300–310.
4. Bardella C, Pollard PJ, Tomlinson I. SDH mutations in cancer. *Biochim Biophys Acta*. 2011;1807(11):1432-1443.
5. Cantor JR, Sabatini DM. Cancer cell metabolism: one hallmark,many faces. *Cancer Discovery.* 2012;2:881–898.
6. Bayley JP, Devilee P, Taschner PEM. The SDH mutation database: an online resource for succinate dehydrogenase sequence variants involved in pheochromocytoma, paraganglioma and mitochondrial complex II deficiency. *BMC Medical Genetics*. 2005;6(39).
7. Ni Y, Zbuk KM, Orloff MS, Waite KA, Eng C. Germline Mutations and Variants in the Succinate Dehydrogenase Genes in Cowden and Cowden-like Syndromes. *Am J Hum Genet*. 2008;83(2):261-268.

8. Kusakabe T, Kawaguchi A, Kawaguchi R, Feigenbaum L, Kimura S. Thyrocyte-specific expression of Cre recombinase in transgenic mice. *Genesis.* 2004; 39:212–216.
9. Ashtekar A, Huk D, Magner A, La Perle K, Jhiang SM, Kirschner LS. Sdhd ablation promotes thyroid tumorigenesis by inducing a stem-like phenotype. *Endocr Relat Cancer*. 2017;24(11):579-591.
10. Nagy R, Sweet K, Eng C. Highly penetrant hereditary cancer syndromes. *Oncogene.* 2004;23:6445–6470.
11. Pringle DR, Yin Z, Parlow AF, Jarjoura D, La Perle KMD, Kirschner LS. Thyroid specific ablation of the Carney Complex gene, PRKAR1A, results in hyperthyroidism and follicular thyroid cancer. *Endocr Relat Cancer*. 2012;19(3): 435–446.
12. Yu W, He X, Ni Y, Ngeow J, Eng C. Cowden syndrome-associated germline SDHD variants alter PTEN nuclear translocation through SRC-induced PTEN oxidation. *Human Molecular Genetics.* 2015;24:142–153.
13. Yeager N, Klein-Szanto A, Kimura S, Di Cristofano A. Pten loss in the mouse thyroid causes goiter and follicular adenomas: insights into thyroid function and Cowden disease pathogenesis. *Cancer Res.* 2007;67:959-66.
14. Gill AJ. Succinate dehydrogenase (SDH)-deficient neoplasia. *Histopathology.* 2018;72:106–116.
15. Vasko V, Espinosa AV, Scouten W, He H, Auer H, de la Chapelle A, Saji M, Ringel MD. Gene expression and functional evidence of epithelial-to-mesenchymal transition in papillary thyroid carcinoma invasion. *Proc Natl Acad Sci USA.* 2007;104:2803-8.

16. Aspuria PJ, Lunt SY, Varemo L, Vergnes L, Gozo M, Beach JA, Nielsen J. Succinate dehydrogenase inhibition leads to epithelial-mesenchymal transition and reprogrammed carbon metabolism. *Cancer and Metabolism.* 2014; 2(21).